Study of the effective cutter radius for end milling of free-form surfaces using a torus milling cutter

Jean-Max Redonnet, Sonia Djebali, Stéphane Segonds, Johanna Senatore, Walter Rubio

Study of the effective cutter radius for end milling of free-form surfaces using a torus milling cutter

Jean-Max REDONNET, Sonia DJEBALI, Stéphane SEGONDS,
Johanna SENATORE and Walter RUBIO

Université de Toulouse, Institut Clément Ader
UPS, 118 rte de Narbonne, 31062 Toulouse France

Computer-Aided Design, vol 45 (6), pp 951-962, 2013
DOI: 10.1016/j.cad.2013.03.002

Abstract

When end milling free-form surfaces using a torus milling cutter, the notion of cutter effective radius is often used to address the procedure for removal of material from a purely geometrical perspective. Using an original analytical approach, the present study establishes a relation enabling the value of this effective radius to be easily computed. The limits of validity of this relation are then discussed and precisely defined.
By way of an illustration, an example of how this relation can be used to generate a numerical tool for analysis of the possibilities for machining free-form surfaces on multi-axis machine-tools is also presented.

Keywords: free-form surface; CNC machine-tool; end-mill; toroidal cutter; effective tool radius; swept curve

Contents

1 Introduction

End milling of free-form surfaces is essentially used to manufacture moulds and dies where it is often extremely costly in terms of production time consumed. From a purely geometrical standpoint, precise modelling of the movements of the cutter and its positioning in relation to the surface are indispensable to be able to propose improvements to boost productivity. From this perspective, an approach commonly adopted is based on notions of effective radius and/or sweep curve. Indeed, good knowledge of these geometrical entities paves the way for a precise analysis of the trace left by the cutter in the workpiece and through that, the quantity of material actually removed.

1.1 Previous works on the effective cutter radius

Tool path planning, optimisation of cutter positioning and non-interference issues are often the focus of research conducted in the field of free-form surface machining on multi-axis machine tools [1]. Among these works, many studies refer to the notion of cutter effective radius. The first to introduce this concept were Vickers and Quan in 1989. In [2], they show how a flat-end mill tilted to the front can be more productive than a ball-end mill. To do so, they introduce the notion of effective radius in the case of the flat-end mill:

$$R_{eff} = \frac{R}{\sin(\phi)}$$

where R is the cutter radius and ϕ its tilt angle in the plane formed by its feed direction and axis of rotation.

The relative efficiency of flat-end mills and ball-end mills is also analysed in [3], [4] and [5]. These works are also based on the effective radius concept to show that, all other parameters being equal, flat-end cutters, when correctly used, produce a lower scallop height than that produced by ball-end cutters. In [4] and [5], the authors also show that flat end mills leave pronounced marks in the feed direction leading to a greater roughness of the surfaces obtained (for the same feed per tooth).

Following these works a number of authors have argued in favour of using torus cutters when milling free-form surfaces. Indeed, torus mills allow a significant effective radius to be retained while avoiding the sharp and unsightly marks left in the workpiece by flat-end mills [6]. Many studies arrive at the same conclusions, whether they adopt a procedure to optimise the cutter position [7,8] or seek rather to eliminate interference [9, 10].

Among the works that address the cutter effective radius concept, those most frequently encountered in the literature utilise the envelope curve concept. For a given cutter position, the envelope curve materialises the trace left by the cutter in the material. In [11], it is approximated, for a torus milling cutter, by the projection of a circle in a plane normal to the feed. In [12], it is given in the implicit form for an APT cutter.

Within the scope of machining simulation [13], many studies use this concept to determine the volume of swarf actually removed by the cutter, but most of these works [14–16] address this issue numerically, which does indeed allow the swept volume to be computed, but precludes an analytical study of the effective cutter radius. The sweep curve and effective cutter radius notions are also largely used in works addressing constant scallop height machining planning. This toolpath planning technique was initially introduced in [17] and [18] using a ball-end cutter. Subsequently it was adapted for a flat-end mill [19, 20] and for the torus milling cutter [21, 22], tools for which the effective radius assumes its full significance.

Analysis of the main studies published in the field shows that most works covering the effective radius of the torus milling cutter rely on geometric approximations (with non-negligible consequences) or use a numerical approach that, compared with an analytical approach, proves to be less flexible and much more time-consuming in computation.

1.2 The present article's contribution

The present article will introduce a new study of the torus milling cutter effective radius. Its originality lies in its totally analytical approach that nevertheless refrains from any geometric approximation. The main result of this work is the definition of a relation authorizing an analytical calculation of the effective cutter radius.

This study is also accompanied by an analysis of this relation and its limits, thus allowing the scope for its validity to be clearly determined.

This is followed by an example in which it is

shown how this relation can be used to define numerical tools potentially useful within the scope of end milling of free-form surfaces on multi-axis machine tools. The aim with this example is not to define a complete procedure to plan tool paths, but simply to emphasise the possibilities offered by using an analytical formula where numerical procedures are usually applied.

The article concludes with a reminder of the main results obtained and some remarks on forthcoming works on this subject.

2 Calculating the effective radius

2.1 Introduction

It will be shown how it is possible to calculate analytically, at the point of cutter/workpiece contact, the effective radius of a torus milling cutter machining a free-form surface on a multi-axis NC machine tool. This calculation is based on two mathematical demonstrations that will be introduced prior to the computation itself.

A torus milling cutter defined by R and r, R being the outer radius of that cutter and r being its torus radius, is considered. The trace left by that cutter in the material at a given instant is a curve that will be referred to as the envelope curve. It is the succession of such envelope curves that forms the envelope surface generated by the cutter movement in the material. At each instant, the envelope curve is defined by $\mathbf{F_t} \cdot \mathbf{n} = 0$, where $\mathbf{F_t}$ is a vector in the cutter feed direction and $\mathbf{n}$ a vector normal to the surface of the cutter.

In what follows in the present study, the vector $\mathbf{F_t}$ will be assumed to be constant for all points of the cutter; this is equivalent to asserting that the cutter moves in translation, at least locally. Moreover, only the part of the envelope curve of the cutter contained in the torus part of the cutter will be considered. Indeed, the great majority of torus milling cutters used in industry are round insert cutters and only that part is active. Also, studying the parts of the envelope curve contained in the cylindrical and discoid portions of the cutter is unproblematic and, even in the case of solid torus milling cutters, these parts of the cutter are normally inactive when removing material, especially when conducting finishing operations.

The two lemmas on which the calculation is based are as follows:

Lemma 1 *Let $\mathcal{P}$ be the mathematical operation for projection along the feed direction $\mathbf{F_t}$ in a plane normal to $\mathbf{F_t}$. Let $\mathbf{T_p}(v)$, be the curve resulting from the projection along $\mathcal{P}$ of the cutter envelope. Let $\mathbf{E}(t)$ be the ellipse resulting from the projection along $\mathcal{P}$ of the cutter centre-torus circle, and $\mathbf{oE}(t)$ an offset exterior to that ellipse with a value equal to the radius of the cutter torus. Then the two curves $\mathbf{T_p}(v)$ and $\mathbf{oE}(t)$ are coincident.*

Lemma 2 *The radius of curvature of a plane offset curve is equal to the radius of curvature of the original curve augmented by the offset value.*

It will thus be shown initially that the projection of the cutter envelope curve in a plane normal to the feed direction $\mathbf{F_t}$ can be defined by an ellipse augmented by an offset equal to the cutter torus radius (section 2.2).

It will then be shown that the radius of curvature of an offset to this ellipse is equal to the radius of curvature of the original ellipse augmented by the offset value (section 2.3).

Based on these results, it will then be possible to calculate analytically the effective radius of the cutter R_{eff} considering the radius of curvature of the ellipse $\mathbf{E}(t)$ to which is added the cutter torus radius the cutter (section 2.4).

All these calculations were verified using the algebraic computation software Maxima [23].

2.2 Demonstration of lemma 1

2.2.1 Statement of the problem

Firstly the projection of the cutter envelope curve in a plane normal to $\mathbf{F_t}$ is considered, then an offset by r of the ellipse defined by the projection of the torus major radius circle of the cutter (centre of the torus tube) in the same plane (Fig. 1 and 2).

The purpose of this demonstration is to show that these two curves coincide.

2.2.2 Definitions

Naming R_t the radius of the cutter torus centre circle ($R_t = R - r$), the toroid surface defining the cutter

in its reference frame can be defined by:

$$\mathbf{T}(u,v) = \begin{pmatrix} (R_t + r\,\cos(v))\cos(u) \\ (R_t + r\,\cos(v))\sin(u) \\ r\,\sin(v) \end{pmatrix} \qquad (1)$$

$$\text{with } u \in [0, 2\pi] \text{ and } v \in \left[-\tfrac{\pi}{2}, 0\right]$$

Let $\mathbf{F}$, be a unit vector in the machining direction $\mathbf{F_t}$:

$$\mathbf{F} = \frac{\mathbf{F_t}}{\|\mathbf{F_t}\|}$$

The trace left by the cutter (envelope curve) can then be defined by $\mathbf{F} \cdot \mathbf{n} = 0$, where $\mathbf{n}$ is the normal to the cutter surface.

Consider the projection along the feed direction $\mathbf{F}$ in a plane P perpendicular to $\mathbf{F}$. Naming a, b and c the coordinates of $\mathbf{F}$, the plane P is expressed by equation :

$$a\,x + b\,y + c\,z = d \qquad \text{with } d \in \mathbb{R}$$

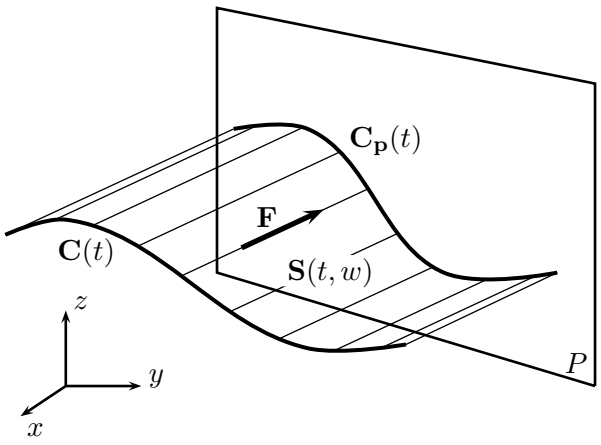

Figure 1: Projection of a parametric curve in a plane

Let $\mathbf{C}(t)$ be a curve defined in three dimensions by:

$$\mathbf{C}(t) = \begin{pmatrix} C_x(t) \\ C_y(t) \\ C_z(t) \end{pmatrix}$$

The curve $\mathbf{C_p}(t)$ resulting from the projection of $\mathbf{C}(t)$ in P along the direction $\mathbf{F}$ is then defined by the intersection of the plane P and the surface defined by $\mathbf{S}(t,w) = \mathbf{C}(t) + f(w)\,\mathbf{F}$ where $f(w)$ is a scalar function of the parameter w defined in $[-\infty, +\infty]$ (Fig. 1). This surface is the ruled surface defined from $\mathbf{C}(t)$ and $\mathbf{F}$. The projected curve $\mathbf{C_p}(t)$ is thus defined by the system:

$$\begin{cases} a\,x + b\,y + c\,z = d \\ x = C_x(t) + a\,f(w) \\ y = C_y(t) + b\,f(w) \\ z = C_z(t) + c\,f(w) \end{cases}$$

where x, y and z represent the three coordinates of the curve $\mathbf{C_p}(t)$.

Resolving this system in relation to x, y, z and $f(w)$, the expression of these coordinates is obtained as a function of t that will be referred to as $C_{px}(t)$, $C_{py}(t)$ and $C_{pz}(t)$:

$$\begin{cases} C_{px}(t) = \frac{-a\,c\,C_z(t) - a\,b\,C_y(t) + c^2\,C_x(t) + b^2\,C_x(t) + a\,d}{c^2+b^2+a^2} \\ C_{py}(t) = \frac{-b\,c\,C_z(t) + c^2\,C_y(t) + a^2\,C_y(t) - a\,b\,C_x(t) + b\,d}{c^2+b^2+a^2} \\ C_{pz}(t) = \frac{b^2\,C_z(t) + a^2\,C_z(t) + c\,(-b\,C_y(t) - a\,C_x(t)) + c\,d}{c^2+b^2+a^2} \end{cases}$$

as also

$$f(w) = \frac{-c\,C_z(t) - b\,C_y(t) - a\,C_x(t) + d}{c^2 + b^2 + a^2}$$

Given that the vector $\mathbf{F}$ is unitary, this gives $a^2 + b^2 + c^2 = 1$, whence the equation for the projected curve:

$$\mathbf{C_p}(t) = \begin{pmatrix} -a\,c\,C_z(t) - a\,b\,C_y(t) + c^2\,C_x(t) + b^2\,C_x(t) + a\,d \\ -b\,c\,C_z(t) + c^2\,C_y(t) + a^2\,C_y(t) - a\,b\,C_x(t) + b\,d \\ b^2\,C_z(t) + a^2\,C_z(t) + c\,(-b\,C_y(t) - a\,C_x(t)) + c\,d \end{pmatrix} \qquad (2)$$

2.2.3 Contextualisation

Within the scope of the present study, the cutter is defined within its own reference frame, the axis coinciding with its axis of rotation. As the cutter is a surface of revolution, whatever the movement of translation driving it, the envelope curve resulting from this movement, defined by $\mathbf{F} \cdot \mathbf{n} = 0$, admits a

plane of symmetry containing the axis z of the reference frame. Furthermore, a projection $\mathcal{P}$ in a plane normal to the feed $\mathbf{F}$ is considered. This projection thus corresponds to a vector contained within the plane of symmetry of the envelope curve. The problem is thus axisymmetric. Consequently, the results obtained in the case of a particular projection (i.e. in a given radial direction) are true whatever the projection $\mathcal{P}$ considered, meaning whatever translation movement drives the cutter. It can thus be considered that the results obtained in the case of a projection along a vector contained in the plane $x = 0$ (or $y = 0$) can be extended to the general case.

A projection $\mathcal{P}$ is chosen whose direction $\mathbf{F}$ is contained in the plane of equation $x = 0$, with coordinate a of $\mathbf{F}$ thus being null. The plane P normal to this projection will then have for equation $b\,y + c\,z = d$ and the coordinates of vector $\mathbf{F}$ are:

$$\mathbf{F} = \begin{pmatrix} 0 \\ b \\ c \end{pmatrix}$$

In what follows in the present demonstration, $b \neq 0$ and $c \neq 0$ will be considered. Indeed, instances where $b = 0$ and $c = 0$ correspond to horizontal or vertical cutter paths that constitute special cases that will be addressed in section 3.2.

Furthermore, as vector $\mathbf{F}$ is unitary, it can be asserted that $b^2 + c^2 = 1$.

Also, in so far as the focus is on curves projected orthogonally in a plane normal to the milling direction, any plane normal to that direction can be chosen without impairing generality. To simplify computation, a plane P passing through the origin is chosen, that is a plane with equation $b\,y + c\,z = 0$. This gives $d = 0$.

Taking these considerations into account, the equation (2) for a curve transformed along projection $\mathcal{P}$ becomes:

$$\mathbf{C_p}(t) = \begin{pmatrix} C_x(t) \\ -b\,c\,C_z(t) + c^2\,C_y(t) \\ b^2\,C_z(t) - b\,c\,C_y(t) \end{pmatrix} \qquad (3)$$

In the following demonstration, will be considered the projection $\mathcal{P}$, defined by equation (3) enabling a curve to be projected in a plane P according to a vector $\mathbf{F}$, with plane P going through the origin and being normal to the vector $\mathbf{F}$ that is contained in the plane of equation $x = 0$.

2.2.4 Demonstration

First of all, the projection $\mathcal{P}$ is applied to the circle $\mathbf{C}(t)$, the cutter torus centre, defined by the equation

$$\mathbf{C}(t) = \begin{pmatrix} R_t\,\cos(t) \\ R_t\,\sin(t) \\ 0 \end{pmatrix} \quad \text{with} \quad t \in [0, 2\pi]$$

Using (3), the orthogonal projection of that circle can be defined in the plane of equation $b\,y + c\,z = 0$. This projection is an ellipse that will be referred to as $\mathbf{E}(t)$, and whose equation is:

$$\mathbf{E}(t) = \begin{pmatrix} R_t\,\cos(t) \\ c^2\,R_t\,\sin(t) \\ -b\,c\,R_t\,\sin(t) \end{pmatrix}$$

In what follows, only the lower part of the ellipse $\mathbf{E}(t)$ will be considered, that is the part defined by $t \in [-\pi, 0]$ (Fig. 2).

The unit vector $\mathbf{nE}(t)$ normal to $\mathbf{E}(t)$ and contained in the plane P can then be defined by:

$$\mathbf{nE}(t) = \frac{\frac{\mathrm{d}\mathbf{E}(t)}{\mathrm{d}t} \times \mathbf{F}}{\left\| \frac{\mathrm{d}\mathbf{E}(t)}{\mathrm{d}t} \times \mathbf{F} \right\|}$$

that is

$$\mathbf{nE}(t) = \frac{1}{\sqrt{b^2 \sin^2(t) + c^2}} \begin{pmatrix} c\,\cos(t) \\ c\,\sin(t) \\ -b\,\sin(t) \end{pmatrix} \qquad (4)$$

Given the previously established restrictions ($c \neq 0$ and $b \neq 0$), this expression is defined whatever $t \in [-\pi, 0]$.

In the plane P, $\mathbf{oE}(t)$ is defined, an offset with value r to the ellipse $\mathbf{E}(t)$:

$$\mathbf{oE}(t) = \mathbf{E}(t) + r\,\mathbf{nE}(t)$$

This curve is expressed as follows:

$$\mathbf{oE}(t) = \begin{pmatrix} \cos(t)\,R_t + \frac{c\,r\,\cos(t)}{\sqrt{b^2 \sin^2(t) + c^2}} \\ c^2\,\sin(t)\,R_t + \frac{c\,r\,\sin(t)}{\sqrt{b^2 \sin^2(t) + c^2}} \\ -b\,c\,\sin(t)\,R_t - \frac{b\,r\,\sin(t)}{\sqrt{b^2 \sin^2(t) + c^2}} \end{pmatrix} \qquad (5)$$

Secondly, the envelope curve is considered, that is the trace left by the cutter in the material at a given instant. For a torus milling cutter whose definition

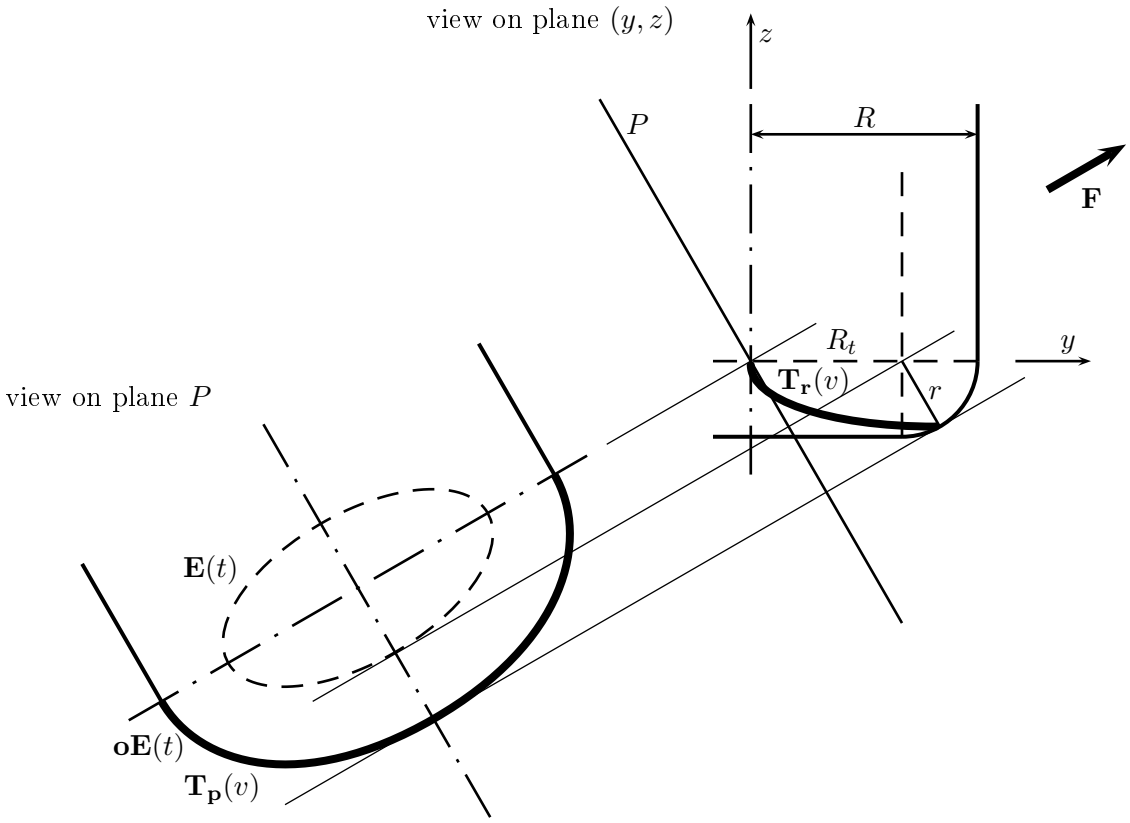

Figure 2: Projection of the envelope curve and the torus centre circle in a plane normal to $\mathbf{F}$

is given by the equation (1), this envelope curve is defined by $\mathbf{F} \cdot \mathbf{nT}(u, v) = 0$, where $\mathbf{nT}(u, v)$ is a vector normal to $\mathbf{T}(u, v)$.

$$\mathbf{nT}(u, v) = \frac{\partial \mathbf{T}(u, v)}{\partial u} \times \frac{\partial \mathbf{T}(u, v)}{\partial v}$$

that is

$$\mathbf{nT}(u, v) = \begin{pmatrix} r\ \cos(u)\ \cos(v)\ (R_t + r\ \cos(v)) \\ r\ \sin(u)\ \cos(v)\ (R_t + r\ \cos(v)) \\ r\ \sin(v)\ (R_t + r\ \cos(v)) \end{pmatrix}$$

with $u \in [0, \pi]$ and $v \in \left[-\frac{\pi}{2}, 0\right]$

The equation $\mathbf{F} \cdot \mathbf{nT}(u, v) = 0$ can then be expressed

$$r\ (c\ \sin(v) + b\ \sin(u)\ \cos(v))\ (R_t + r\ \cos(v)) = 0 \tag{6}$$

whence it can be deduced that

$$\sin(u) = -\frac{c\ \sin(v)}{b\ \cos(v)} \tag{7}$$

for $v \in \left]-\frac{\pi}{2}, 0\right]$. Section 3.2 adresses the case where $v = -\frac{\pi}{2}$. In what follows in the demonstration, it will be considered that $-\frac{\pi}{2} < v \leqslant 0$.

Using this relation (7) in the expression of $\mathbf{T}(u, v)$ — equation (1) — the equation of the envelope curve, referred to as $\mathbf{T_r}(v)$, is obtained:

$$\mathbf{T_r}(v) = \begin{pmatrix} \sqrt{1 - \frac{c^2 \sin^2(v)}{b^2 \cos^2(v)}}\ (R_t + r\ \cos(v)) \\ -\frac{c\ \sin(v)\ (R_t + r\ \cos(v))}{b\ \cos(v)} \\ r\ \sin(v) \end{pmatrix}$$

for $u \in \left[0, \frac{\pi}{2}\right]$, and

$$\mathbf{T_r}(v) = \begin{pmatrix} -\sqrt{1 - \frac{c^2 \sin^2(v)}{b^2 \cos^2(v)}}\ (R_t + r\ \cos(v)) \\ -\frac{c\ \sin(v)\ (R_t + r\ \cos(v))}{b\ \cos(v)} \\ r\ \sin(v) \end{pmatrix}$$

for $u \in \left[\frac{\pi}{2}, \pi\right]$. As the curve $\mathbf{T_r}(v)$ is symmetrical in relation to the plane of equation $x = 0$ corresponding to parameter $u = \frac{\pi}{2}$, only the part defined by $0 \leqslant u \leqslant \frac{\pi}{2}$ will be considered in what follows, with the same reasoning being applicable by symmetry for the part defined by $\frac{\pi}{2} \leqslant u \leqslant \pi$.

As previously, using (3) the projection of that curve can be defined in the plane P. Thus the curve $\mathbf{T_p}(v)$ can be obtained:

$$\mathbf{T_p}(v) = \begin{pmatrix} \sqrt{1 - \frac{c^2 \sin^2(v)}{b^2 \cos^2(v)}}\ (R_t + r\ \cos(v)) \\ -\frac{c^3\ \sin(v)\ (R_t + r\ \cos(v))}{b\ \cos(v)} - b\,c\,r\ \sin(v) \\ \frac{c^2\ \sin(v)\ (R_t + r\ \cos(v))}{\cos(v)} + b^2\,r\ \sin(v) \end{pmatrix} \quad (8)$$

The problem posed can thus be reduced to showing that $\mathbf{oE}(t) = \mathbf{T_p}(v)$.

By identifying the coordinates of these two curves (equations 5 and 8) member by member, 3 equations are obtained:

$$\cos(t)\,R_t + \frac{c\,r\ \cos(t)}{\sqrt{b^2 \sin^2(t) + c^2}} = \sqrt{1 - \frac{c^2 \sin^2(v)}{b^2 \cos^2(v)}}\ (R_t + r\ \cos(v)) \quad (9)$$

$$c^2\ \sin(t)\,R_t + \frac{c\,r\ \sin(t)}{\sqrt{b^2 \sin^2(t) + c^2}} = -\frac{c^3\ \sin(v)\ (R_t + r\ \cos(v))}{b\ \cos(v)} - b\,c\,r\ \sin(v) \quad (10)$$

$$-b\,c\ \sin(t)\,R_t - \frac{b\,r\ \sin(t)}{\sqrt{b^2 \sin^2(t) + c^2}} = \frac{c^2\ \sin(v)\ (R_t + r\ \cos(v))}{\cos(v)} + b^2\,r\ \sin(v) \quad (11)$$

Analysing these equations, it clearly emerges that the last two, (10) and (11), are equivalent. Indeed, by multiplying each term of equation (10) by $-b/c$, equation (11) is obtained.

To show that the two curves are equal, all one needs to do is find a change in variable linking t and v such that the equation of one of the two curves can be transformed into the equation of the other curve.

To do so, the terms on R_t and r between the first equation (9) and one of the two others (for example (10)) are identified member by member.

From equation (9), identifying the terms on R_t, the following is obtained:

$$\cos(t) = \sqrt{1 - \frac{c^2\ \sin^2(v)}{b^2\ \cos^2(v)}} \quad (12)$$

and identifying the terms on r, this gives:

$$\frac{c\,\cos(t)}{\sqrt{b^2 \sin^2(t) + c^2}} = \sqrt{1 - \frac{c^2 \sin^2(v)}{b^2 \cos^2(v)}}\,\cos(v) \quad (13)$$

which, after simplification (see 5), results in returning to equation (5):

$$\cos(t) = \sqrt{1 - \frac{c^2\ \sin^2(v)}{b^2\ \cos^2(v)}}$$

From equation (10), identifying the terms on R_t, the following is obtained:

$$c^2\ \sin(t) = -\frac{c^3\ \sin(v)}{b\ \cos(v)}$$

whence it can be deduced

$$\begin{aligned} \sin(t) &= -\frac{c\ \sin(v)}{b\ \cos(v)} \\ 1 - \cos^2(t) &= \frac{c^2\ \sin^2(v)}{b^2\ \cos^2(v)} \end{aligned}$$

which results in returning to equation (12):

$$\cos(t) = \sqrt{1 - \frac{c^2\ \sin^2(v)}{b^2\ \cos^2(v)}}$$

From this same equation (10), identifying the terms on r, the following is obtained:

$$\frac{c\ \sin(t)}{\sqrt{b^2\ \sin^2(t) + c^2}} = -\left(\frac{c^3}{b}\ \sin(v) + b\,c\ \sin(v)\right) \quad (14)$$

which, after simplification (see 5), again gives the equation (12):

$$\cos(t) = \sqrt{1 - \frac{c^2\ \sin^2(v)}{b^2\ \cos^2(v)}}$$

Identification of the terms on R_t and r for equations (9) and (10) thus leads to the same relation (12) linking parameters t and v. Using this relation as a change in variable, it proves possible to pass from equation (5) to equation (8). There is thus a change in variable to go from one curve to the other. This leads to concluding that curves $\mathbf{T_p}(v)$ and $\mathbf{oE}(t)$ coincide.

2.2.5 Conclusion

It was shown that in the case of a projection $\mathcal{P}$ in a plane going through the origin and along a vector $\mathbf{F}$ contained in the plane of equation $x = 0$, the two curves $\mathbf{T_p}(v)$ and $\mathbf{oE}(t)$ coincide. As the problem is axisymmetric, what is true in this instance is also true whatever the plane of projection, provided that the projection is made along a normal to that plane. In the case of a translation movement, the curve resulting from the projection plane of the trace left by the cutter thus coincides with the curve parallel to the ellipse, located at a distance r outside the latter that itself results from the projection of the torus centre circle.

2.3 Demonstration of lemma 2

This demonstration's objective is to show that the radius of curvature of a plane offset curve is equal to the radius of curvature of the original curve augmented by the value of the offset.

Let $\mathbf{C}$ be a plane curve whose parameters are set by its curvilinear abscissa s. Let $\mathbf{C_o}$ be an offset curve derived from $\mathbf{C}$:

$$\mathbf{C_o} = \mathbf{C} + r\,\mathbf{n}$$

where r is the scalar value of the offset and $\mathbf{n}$ the unit normal to $\mathbf{C}$ oriented towards the centre of curvature.

Deriving the previous expression in relation to the curvilinear abscissa s, the following is obtained:

$$\frac{\mathrm{d}\mathbf{C_o}}{\mathrm{d}s} = \frac{\mathrm{d}\mathbf{C}}{\mathrm{d}s} + r\,\frac{\mathrm{d}\mathbf{n}}{\mathrm{d}s}$$

where $\dfrac{\mathrm{d}\mathbf{C}}{\mathrm{d}s}$ is the unit vector $\mathbf{t}$, tangent to $\mathbf{C}$.

Calling s_o the curvilinear abscissa of the curve $\mathbf{C_o}$ one obtains:

$$\frac{\mathrm{d}\mathbf{C_o}}{\mathrm{d}s_o}\,\frac{\mathrm{d}s_o}{\mathrm{d}s} = \mathbf{t} + r\,\frac{\mathrm{d}\mathbf{n}}{\mathrm{d}s}$$

Frenet formulae give:

$$\frac{\mathrm{d}\mathbf{n}}{\mathrm{d}s} = \tau\,\mathbf{b} - \kappa\,\mathbf{t}$$

where κ is the curvature of $\mathbf{C}$ at the point considered.

As the curve $\mathbf{C}$ is plane, twisting τ is null and thus:

$$\frac{\mathrm{d}\mathbf{n}}{\mathrm{d}s} = -\kappa\,\mathbf{t}$$

giving:

$$\frac{\mathrm{d}\mathbf{C_o}}{\mathrm{d}s_o}\,\frac{\mathrm{d}s_o}{\mathrm{d}s} = \mathbf{t} - r\,\kappa\,\mathbf{t} = (1 - r\,\kappa)\,\mathbf{t} \qquad (15)$$

By definition $\frac{\mathrm{d}\mathbf{C_o}}{\mathrm{d}s_o}$ is the unit vector tangent to $\mathbf{C_o}$. As the curve $\mathbf{C_o}$ is the offset of $\mathbf{C}$, for a given value of s, both curves have the same tangent. Thus

$$\frac{\mathrm{d}\mathbf{C_o}}{\mathrm{d}s_o} = \mathbf{t}$$

Whence, in (15) :

$$\mathbf{t}\,\frac{\mathrm{d}s_o}{\mathrm{d}s} = (1 - r\,\kappa)\,\mathbf{t}$$

which can be simplified:

$$\frac{\mathrm{d}s_o}{\mathrm{d}s} = 1 - r\,\kappa \qquad (16)$$

Moreover, the Frenet formulae give:

$$\frac{\mathrm{d}\mathbf{t}}{\mathrm{d}s_o} = \kappa_o\,\mathbf{n}$$

whence

$$\frac{\mathrm{d}\mathbf{t}}{\mathrm{d}s_o} = \frac{\mathrm{d}\mathbf{t}}{\mathrm{d}s}\,\frac{\mathrm{d}s}{\mathrm{d}s_o}$$

or

$$\frac{\mathrm{d}\mathbf{t}}{\mathrm{d}s} = \kappa\,\mathbf{n}$$

and, according to (16)

$$\frac{\mathrm{d}s}{\mathrm{d}s_o} = \frac{1}{1 - r\,\kappa}$$

Thus

$$\kappa_o\,\mathbf{n} = \kappa\,\mathbf{n}\,\frac{1}{1 - r\,\kappa}$$

Whence it can be deduced that:

$$\kappa_o = \frac{\kappa}{1 - r\,\kappa} \qquad (17)$$

Let ρ be the radius of curvature of $\mathbf{C}$ and ρ_o the radius of curvature of $\mathbf{C_o}$. These magnitudes are related to curvatures κ and κ_o by:

$$\rho = \frac{1}{\kappa} \quad \text{et} \quad \rho_o = \frac{1}{\kappa_o}$$

Whence, in (17) :

$$\frac{1}{\rho_o} = \frac{\frac{1}{\rho}}{1 - \frac{r}{\rho}}$$

which can be expressed:

$$\frac{1}{\rho_o} = \frac{1}{\rho - r}$$

and finally:

$$\rho_o = \rho - r$$

In the case of a plane curve $\mathbf{C}$, the radius of curvature of an offset to $\mathbf{C}$ is equal to the radius of curvature of $\mathbf{C}$ reduced by the algebraic value of the offset. It can therefore be concluded that in the case of an offset remoter from the centre of curvature than the original curve, the radius of curvature of the offset curve will be equal to the radius of curvature of the initial curve increased by the absolute value of the offset.

2.4 Calculating the effective radius

During milling (Fig. 3), the cutter axis coincides with the z-axis of the reference frame and the x and y axes of the reference frame are set as previously (see section 2.2.3), i.e. the feed direction $\mathbf{F_t}$ is contained in the plane $x = 0$.

Furthermore, let $\mathbf{D}$ be the unit vector contained in the plane (x, y) that indicates the direction of the greatest slope at the cutter/workpiece point of contact (point $\mathbf{C_c}$). The normal to the surface at that point ($\mathbf{n_{cc}}$) is then contained in the plane $(\mathbf{D}, z)$.

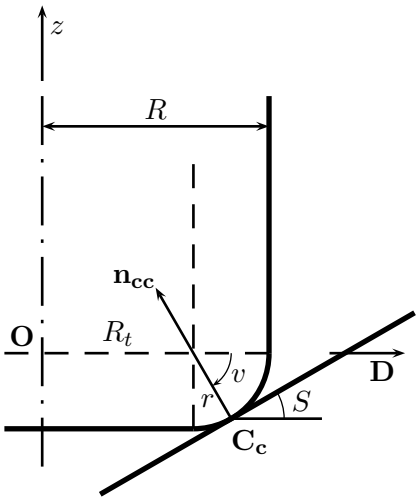

Figure 3: Defining angle S

S designates the slope of the surface machined at the cutter/workpiece point of contact $\mathbf{C_c}$. This angle S is contained in the plane $(\mathbf{D}, z)$. Only the case where $S \neq 0$ will be considered in the present calculation. Indeed, milling in a direction contained within the plane (x, y) constitutes a special case that will be addressed in section 3.2. Thus $S > 0$.

This angle S is also that between the cutter axis z and the normal to the surface at the point of contact $\mathbf{n_{cc}}$. The vector $\mathbf{n_{cc}}$ can be expressed in the form:

$$\mathbf{n_{cc}} = -\sin(S)\,\mathbf{D} + \cos(S)\,\mathbf{z} \tag{18}$$

α will designate the angle separating vector $\mathbf{D}$ of the y-axis. The following calculations will be limited to the case where $-\frac{\pi}{2} < \alpha < \frac{\pi}{2}$. Where $\alpha = \pm\frac{\pi}{2}$, the direction with the greatest slope $\mathbf{D}$ is perpendicular to the feed direction $\mathbf{F}$. These values correspond to special cases that will be studied in section 3.2.

In the reference frame $(\mathbf{O}, x, y)$ the vector $\mathbf{D}$ can be expressed:

$$\mathbf{D} = \sin(\alpha)\,\mathbf{x} + \cos(\alpha)\,\mathbf{y} \tag{19}$$

Thus, in the reference frame $(\mathbf{O}, x, y, z)$, the vector $\mathbf{n_{cc}}$ can be expressed:

$$\mathbf{n_{cc}} = \begin{pmatrix} -\sin(S)\ \sin(\alpha) \\ -\sin(S)\ \cos(\alpha) \\ \cos(S) \end{pmatrix} \tag{20}$$

Besides, for each point $\mathbf{C_c}$, the vector $\mathbf{F}$ is determined such that it belongs to the plane tangent to the surface at this point (Fig. 4). In the reference frame $(\mathbf{O}, x, y, z)$, $\mathbf{F}$ can be expressed in the form :

$$\mathbf{F} = \begin{pmatrix} 0 \\ \cos(\psi) \\ \sin(\psi) \end{pmatrix} \tag{21}$$

where ψ designates the angle formed by vector $\mathbf{F}$ and its projection in the plane (x, y). This angle is contained in the plane made by vectors z and y.

To obtain a displacement of the cutter tangent to the surface at the cutter/workpiece point of contact (point $\mathbf{C_c}$), the curve defined by the trace left by the cutter in the material, referred to as the envelope curve, verifies the equation $\mathbf{F} \cdot \mathbf{n_{cc}} = 0$. Using (20) and (21) in this equation, the following is obtained:

$$-\cos(\psi)\ \sin(S)\ \cos(\alpha) + \sin(\psi)\ \cos(S) = 0$$

This gives, for each cutter contact point

$$\tan(\psi) = \tan(S)\ \cos(\alpha) \tag{22}$$

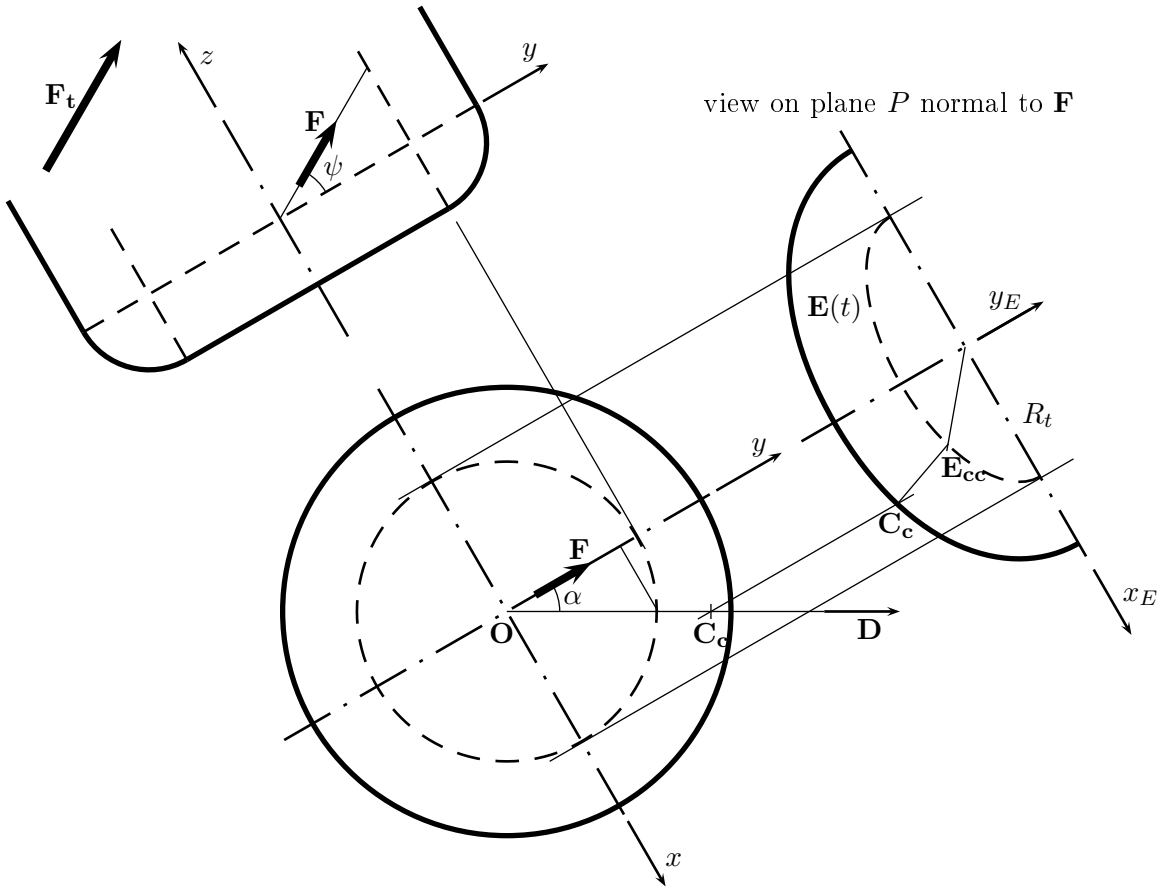

Figure 4: Definition of elements used to calculate the effective radius R_{eff}

In further calculations, only the cases where $0 < \psi < \frac{\pi}{2}$ are considered. Cases where $\psi = 0$ and $\psi = \frac{\pi}{2}$ correspond to special instances that will be studied in section 3.2 (indeed, for $\psi = 0$ the cutter moves horizontally and for $\psi = \frac{\pi}{2}$, it moves vertically).

In its own reference $(\mathbf{O}; x_E, y_E)$, an ellipse is defined by the parametric equation:

$$\mathbf{E}(t) = \begin{pmatrix} \mu \cos(t) \\ \eta \sin(t) \\ 0 \end{pmatrix} \tag{23}$$

where values μ and η represent respectively the semi-major axis and the semi-minor axis of the ellipse $\mathbf{E}(t)$.

In the case of the ellipse resulting from projection of the torus centre circle of radius R_t, in a plane normal to $\mathbf{F}$ (Fig. 4), values μ and η are defined by:

$$\begin{cases} \mu &= R_t \\ \eta &= R_t \sin(\psi) \end{cases} \tag{24}$$

Using the fact that:

$$\sin(\psi) = \frac{\tan(\psi)}{\sqrt{1 + \tan^2(\psi)}}$$

and equation (22) in equation (24), the value of the semi-minor axis η can be expressed by:

$$\eta = R_t \frac{\tan(S)\cos(\alpha)}{\sqrt{1 + \tan^2(S)\cos^2(\alpha)}} \tag{25}$$

In its own plane, the ellipse $\mathbf{E}(t)$ is thus defined by:

$$\mathbf{E}(t) = \begin{pmatrix} R_t \cos(t) \\ R_t \frac{\tan(S)\cos(\alpha)}{\sqrt{1+\tan^2(S)\cos^2(\alpha)}} \sin(t) \\ 0 \end{pmatrix} \tag{26}$$

The radius of curvature of a parametric curve

$\mathbf{C}(t)$ is defined by:

$$\rho_C = \frac{\left\| \frac{\mathrm{d}\mathbf{C}(t)}{\mathrm{d}t} \right\|^3}{\left\| \frac{\mathrm{d}\mathbf{C}(t)}{\mathrm{d}t} \times \frac{\mathrm{d}^2\mathbf{C}(t)}{\mathrm{d}t^2} \right\|}$$

From equation (23), the following can be calculated:

$$\frac{\mathrm{d}\mathbf{E}(t)}{\mathrm{d}t} = \begin{pmatrix} -\mu\,\sin(t) \\ \eta\,\cos(t) \\ 0 \end{pmatrix}$$

and

$$\frac{\mathrm{d}^2\mathbf{E}(t)}{\mathrm{d}t^2} = \begin{pmatrix} -\mu\,\cos(t) \\ -\eta\,\sin(t) \\ 0 \end{pmatrix}$$

The radius of curvature of the ellipse $\mathbf{E}(t)$ is thus equal to:

$$\rho_E = \frac{\left(\mu^2 \sin^2(t) + \eta^2 \cos^2(t)\right)^{3/2}}{\eta\,\mu}$$

and is only defined for $\eta \neq 0$ and $\mu \neq 0$. Now, according to equations (24), $\mu = 0$ implies $R_t = 0$, which cannot be and $\eta = 0$ implies $\psi = 0$. The case where ψ is null corresponds to machining in the plane (x, y) (Fig. 4) which is equivalent to saying that $S = 0$ (Fig. 3) or $\alpha = \pm\frac{\pi}{2}$ (cf. equation (22)); now, as has already been stated, these instances will be analysed in section 3.2.

The radius of curvature of the ellipse is thus given by:

$$\begin{aligned} \rho_E &= \frac{\left(\mu^2\,\left(1-\cos^2(t)\right) + \eta^2\cos^2(t)\right)^{3/2}}{\eta\,\mu} \\ &= \frac{\mu^2}{\eta}\left(1 - \cos^2(t) + \frac{\eta^2}{\mu^2}\cos^2(t)\right)^{3/2} \\ &= \frac{\mu^2}{\eta}\left(1 + \cos^2(t)\,\left(\frac{\eta^2}{\mu^2} - 1\right)\right)^{3/2} \end{aligned} \quad (27)$$

Equation (27) can be used to calculate the radius of curvature of the ellipse $\mathbf{E}(t)$ as a function of the parameter t of that curve. Let $\mathbf{E_{cc}}$ be the point of that ellipse corresponding to the point of contact $\mathbf{C_c}$ (Fig. 4). To determine the radius of curvature of $\mathbf{E}(t)$ at point $\mathbf{E_{cc}}$, the value of parameter t at that point has to be known. To find it, equation (12) is used again. In this equation b and c are the coordinates of the unit feed vector $\mathbf{F}$ and can be expressed by $c = \sin(\psi)$ and $b = \cos(\psi)$ (see equation 21 and Fig. 4). In addition, at point $\mathbf{C_c}$, the value of parameter v is given by $v = -\frac{\pi}{2} + S$ (Fig. 3), whence it can be deduced that $\sin(v) = -\cos(S)$ and $\cos(v) = \sin(S)$. Applying these considerations to equation (12), the following is obtained:

$$\cos(t) = \sqrt{1 - \frac{\sin^2(\psi)\,\cos^2(S)}{\cos^2(\psi)\,\sin^2(S)}}$$

whence it transpires naturally that:

$$\cos(t) = \sqrt{1 - \frac{\tan^2(\psi)}{\tan^2(S)}}$$

Now, according to equation (22),

$$\frac{\tan(\psi)}{\tan(S)} = \cos(\alpha)$$

It can therefore be confirmed that at point $\mathbf{E_{cc}}$, there is $\cos(t) = \sin(\alpha)$. Using this result in equation (27) giving the radius of curvature of the ellipse, the radius of curvature ρ_E at that point can be expressed:

$$\rho_E = \frac{\mu^2}{\eta}\left(1 + \sin^2(\alpha)\,\left(\frac{\eta^2}{\mu^2} - 1\right)\right)^{3/2}$$

Using expressions of μ and η established in equations (24) and (25), the expression of ρ_E becomes:

$$\begin{aligned} \rho_E &= \frac{R_t^2}{\frac{R_t\,\tan(S)\,\cos(\alpha)}{\sqrt{1+\tan^2(S)\,\cos^2(\alpha)}}}\left(1 + \sin^2(\alpha)\left(\frac{\left(\frac{R_t\,\tan(S)\,\cos(\alpha)}{\sqrt{1+\tan^2(S)\,\cos^2(\alpha)}}\right)^2}{R_t^2} - 1\right)\right)^{3/2} \\ &= \frac{R_t\sqrt{1+\tan^2(S)\cos^2(\alpha)}}{\tan(S)\,\cos(\alpha)}\left(1 + \sin^2(\alpha)\left(\frac{\tan^2(S)\,\cos^2(\alpha)}{1+\tan^2(S)\cos^2(\alpha)} - 1\right)\right)^{3/2} \end{aligned}$$

$$\begin{aligned}\rho_E &= \frac{R_t\sqrt{1+\tan^2(S)\cos^2(\alpha)}}{\tan(S)\ \cos(\alpha)}\left(1-\frac{\sin^2(\alpha)}{1+\tan^2(S)\cos^2(\alpha)}\right)^{3/2}\\ &= \frac{R_t}{\tan(S)\ \cos(\alpha)}\frac{\left(\tan^2(S)\cos^2(\alpha)+\cos^2(\alpha)\right)^{3/2}}{1+\ \tan^2(S)\cos^2(\alpha)}\\ &= \frac{R_t\cos^2(\alpha)\ \left(1+\tan^2(S)\right)^{3/2}}{\tan(S)\left(1+\ \tan^2(S)\cos^2(\alpha)\right)}\end{aligned}$$

Given that $1+\tan^2(S)=\frac{1}{\cos^2(S)}$, it can stated that:

$$\rho_E = \frac{R_t\cos^2(\alpha)}{\cos^3(S)\ \tan(S)\left(1+\ \tan^2(S)\cos^2(\alpha)\right)}$$

Also, given the restrictions established on α and S (that is $-\frac{\pi}{2}<\alpha<\frac{\pi}{2}$ and $S\neq 0$), this expression can be simplified as:

$$\rho_E = \frac{R_t\cos^2(\alpha)}{\cos^2(\alpha)\sin^3(S)+\cos^2(S)\ \sin(S)} \qquad (28)$$

or again:

$$\rho_E = \frac{R_t\cos^2(\alpha)}{\sin(S)\left(1-\sin^2(\alpha)\sin^2(S)\right)} \qquad (29)$$

This expression allows the radius of curvature of the ellipse $\mathbf{E}(t)$ resulting from the projection of the torus major radius circle of the cutter in a plane normal to the feed direction to be calculated, and this for the torus centre point of that curve corresponding to the point of contact with the machined surface.

Based on lemma 2 applied to the ellipse, the radius of curvature R_{eff} on $\mathbf{C_c}$ can be expressed by:

$$R_{eff} = \frac{(R-r)\ \cos^2(\alpha)}{\sin(S)\left(1-\sin^2(\alpha)\sin^2(S)\right)}+r \qquad (30)$$

This expression can be used to calculate the effective radius of the cutter at the cutter/workpiece point of contact in the case of end milling of a free-form surface with a torus milling cutter moving in translation on a multi-axis CNC machine.

3 Discussion

3.1 Analysis of the expression of effective radius

In relation (30), angle α, characterising the machining direction projected in the plane (x,y), only enters into expressions $\cos^2(\alpha)$ and $\sin^2(\alpha)$. It can thus be asserted that all other parameters being equal, the value of the effective radius is the same for values α and $\alpha+\pi$. This is equivalent to saying that for a given point, the values of the effective radius are the same whether up milling or climb milling in a diametrically opposite direction. This result is unsurprising in so far as the study of the effective radius is based on a projection in a plane normal to the machining direction.

Moreover, analysis of the relation (30) shows that for $\alpha=\pm\frac{\pi}{2}$, $R_{eff}=r$ obtains, which constitutes the minimum value of the effective radius for a torus milling cutter. Its maximum value, which is theoretically infinite (horizontal machining) is approached when α tends towards 0 and when S tends towards 0.

3.2 Study into limits of validity of the expression of the effective radius

Relation (30) affords an analytical calculation of the effective radius of the cutter at the cutter/workpiece point of contact when machining a free-form surface with a torus milling cutter. It should, however, be recalled here what precisely is the framework of validity for this relation. Firstly, this relation is only valid at the cutter/workpiece point of contact. Indeed, many relations established during computation — (20) and following — are only valid at this point.

The framework of validity of relation (30) is also bounded by the hypotheses adopted during calculation. The most restrictive of these hypotheses is that the feed vector $\mathbf{F}$ is constant at any point of the cutter. As stated previously, this means that locally at least, the cutter is moved by simple translation. Application-wise, this is always true on 3-axis NC machines. For 4- and 5- axis NC machines, this may be true for portions of the paths but this relation cannot be used systematically. In particular, when the axes of rotation of the machine are activated, the relative movement of the cutter in relation to the workpiece comprises a translation and a rotation. In this case, the feed rate cannot be represented by the same vector $\mathbf{F}$ for all points of the cutter.

During the demonstration, restrictions were stated as to the value of components b and c of the feed vector $\mathbf{F}$ (section 2.2.3), on the value of parameter v (section 2.2.4) and the values of angles S, α and ψ (section 2.4). Thus, relation (30) is only demonstrable if $b \neq 0$, $c \neq 0$, $v \neq -\frac{\pi}{2}$, $S \neq 0$, $\alpha \neq \pm\frac{\pi}{2}$, $\psi \neq 0$ and $\psi \neq \frac{\pi}{2}$. Analysis of the mathematical and technological context shows that these different exceptional cases overlap. Indeed, these special cases correspond to quite specific machining configurations. Each of these special configurations will now be analysed, bearing in mind that in all cases, it was possible, during the demonstration, to postulate that $a = 0$ without losing in generality (section 2.2.3):

- Machining of a locally plane surface at the cutter / workpiece point of contact (point $\mathbf{C_c}$): in this instance, vector $\mathbf{F}$ is parallel to the plane (x, y) and point $\mathbf{C_c}$ is located on the lower limit of the torus part of the cutter. Then $c = 0$, $v = -\frac{\pi}{2}$, $S = 0$ (Fig. 3) and $\psi = 0$ (Fig. 4) obtain. Projection of the cutter envelope curve in a plane normal to feed is then a straight line parallel to the plane (x, y), corresponding to a null curvature. In all the other machining configurations, $v \neq -\frac{\pi}{2}$ and $S \neq 0$ necessarily apply. $c \neq 0$ and $\psi \neq 0$ also apply in all the other machining configurations, except for the case of milling perpendicular to the direction of the greatest slope ($\alpha = \pm\frac{\pi}{2}$).

- Machining perpendicular to the direction of the greatest slope. In this instance $c = 0$ and $\alpha = \pm\frac{\pi}{2}$ apply (see Fig. 3 with a machining direction perpendicular to the plane $(\mathbf{D}, z)$ for the machining configuration and Fig. 4 to define angle α). Projection in a plane normal to the feed of the cutter envelope curve is then an arc of circle corresponding to the torus part of the cutter and the effective machining radius is equal to the torus radius r. In all other machining configurations, $\alpha \neq \pm\frac{\pi}{2}$ necessarily obtains.

- Machining along axis z. $b = 0$ and $\psi = \frac{\pi}{2}$ will then apply. This instance could possibly arise when milling vertically with a round insert cutter. The cutter/workpiece point of contact would then be located on the upper limit of the torus part ($v = 0$) and in this case the effective radius of the cutter could be considered to be equal to its outside radius R. Nevertheless, such machining conditions are extremely unfavourable in terms of cutting quality and cutter lifetime and are consequently never applied industrially. However, in all the other machining configurations, $b \neq 0$ and $\psi \neq \frac{\pi}{2}$ will necessarily apply.

The hypotheses adopted during calculation thus correspond to borderline cases that can be managed regardless of the effective radius. While it is appropriate to take them into account when developing tools based on relation (30), this should not be an obstacle to implementation.

4 Example of an application

4.1 Introduction

Determining the effective radius of the cutter at the cutter/workpiece point of contact through a simple analytical formula as with the one established in relation (30) offers many advantages. Indeed, despite the imposed limits established in section 3.2, this result offers the perspective of multiple applications that will be further developed in forthcoming publications. Using an analytical formula is always rapider than a numerical procedure. Calculation of the effective radius by an analytical formula instead of the numerical procedures generally used means applications that were hitherto considered to be hard to contemplate can be developed. For example, thanks to the relation established in (30), an application was readily developed providing a detailed mapping of

the effective radius of the tool over the entire surface almost instantaneously.

This mapping tool was then used to conduct a study into the comparative effectiveness of a ball end mill and a torus milling cutter with the same radius when machining a free-form surface from an industrial environment on a 3-axis NC machine tool.

This surface, relating to a boat propeller measuring 393 mm in diameter (Fig. 5), is the extrados of the blade (Fig. 6).

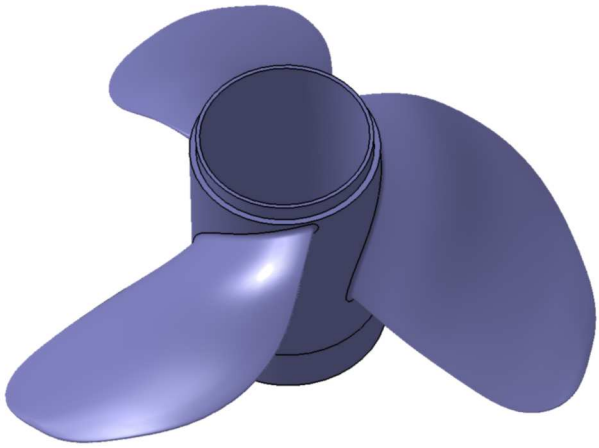

Figure 5: Boat propeller

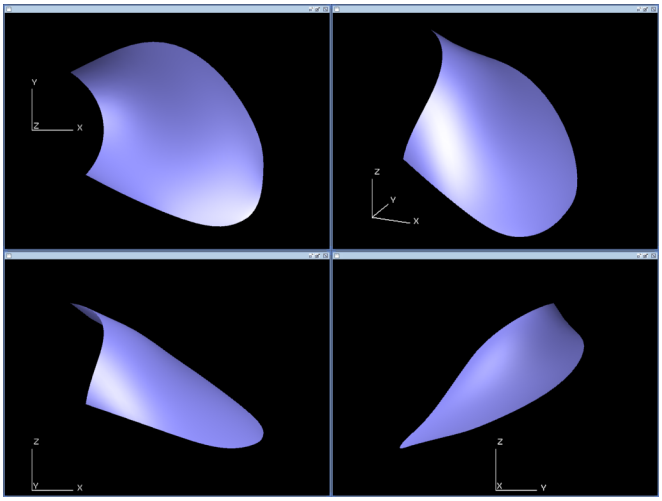

Figure 6: Extrados of a blade

Whatever the tool path planning strategy envisaged (parallel planes, isoparametrics, iso-scallop) the step over distance (defined in section 4.2) must respect the maximum scallop height.

Firstly, it should be recalled that, the step over distance at a point is directly related to the cutter effective radius and, for a given scallop height, that distance has a significant impact on productivity. In what follows, it will be shown how, compared with the results obtained using a ball-end mill, using a torus end cutter can be advantageous in some areas of the workpiece and disadvantageous in others. It will also be seen how the simplicity of the expression established in (30) allows this analysis to be conducted in an extremely short time.

4.2 Relation between step over distance and effective radius

Whatever the tool path planning strategy used, in order to position the cutter so as to respect the maximum scallop height at a given point of the toolpath, the distance d defining its position in the plane perpendicular to the feed direction must first have been calculated (Fig. 7). Subsequently, the step over distance s_{od} can be readily determined as it is directly related to d by angle γ characterising the local inclination of the surface in a plane normal to the machining direction. Showing that the step over distance is directly related to the cutter effective radius is thus equivalent to showing that distance d depends directly on that effective radius.

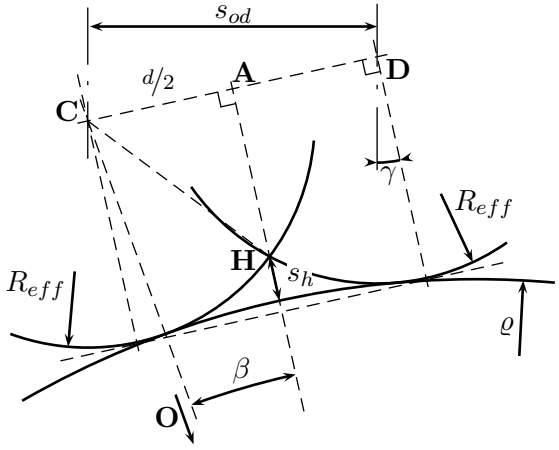

Figure 7: Calculating the step over distance

To calculate the value of d it is assumed that the curvature of surface ϱ (considered in a plane normal to the feed direction) and the cutter effective radius R_{eff} are constant locally. The triangle made by the centre of curvature of the surface called **O**, and points **C** and **H** (Fig. 7) is considered. For this

triangle, the following can be stated:

$$R_{eff}^2 = (R_{eff} + \varrho)^2 + (\varrho + s_h)^2 - 2(R_{eff} + \varrho)(\varrho + s_h)\cos(\beta)$$

where β is the angle between vectors **OC** and **OH**.

Moreover, in triangle (**OAC**), the following applies:

$$\frac{d}{2} = (\varrho + R_{eff})\sin(\beta)$$

Stating $t = \tan^2\left(\frac{\beta}{2}\right)$, the following is obtained:

$$\begin{cases} R_{eff}^2 = (R_{eff} + \varrho)^2 + (\varrho + s_h)^2 - 2(R_{eff} + \varrho)(\varrho + s_h)\frac{1-t^2}{1+t^2} \\ \frac{d}{2} = (\varrho + R_{eff})\frac{2t}{1+t^2} \end{cases}$$

Resolution of this system of equations gives:

$$d = \frac{\sqrt{\left(4\,R_{eff}^2 + 4\,\varrho\,R_{eff} - 2\,s_h\,\varrho - {s_h}^2\right)\,(2\,\varrho + s_h)\,s_h}}{\varrho + s_h} \tag{31}$$

This expression shows that the distance d is indeed directly related to the effective radius R_{eff}, especially considering that s_h can be neglected in relation to the other magnitudes. The step over distance s_{od} thus depends directly on the effective radius R_{eff}. Now, for a given scallop height value (the acceptable tolerance on the surface), the increase in step over distance allows for significant gains in productivity. Consequently, it can be said that this increase in the effective radius of the cutter has a direct impact on productivity.

4.3 Comparison methodology

A seen previously (section 3.1), the effective radius value can vary between the torus radius r in the case of a path perpendicular to the direction of the greatest slope, and a value that tends to infinity for horizontal milling. Given the relation between effective radius cutter and step over distance, it is clear that where the effective radius equals r, using a ball-end cutter instead of a torus milling cutter will allow for greater productivity. However, the closer the path becomes to being horizontal in the direction of the greatest slope, the more the torus milling cutter will prove to be more effective as compared with a ball-end mill of the same diameter. It therefore seems useful to be able to determine, for a given surface, the zones where the torus milling cutter is more effective than the ball-end cutter and vice-versa.

For the ball-end cutter, the effective radius is always equal to its nominal radius R, whatever the feed direction and slope of the surface.

For the torus milling cutter, calculation of the effective radius with the formula established in (30) requires knowledge of the slope of the surface at the point considered and the angle formed by the direction of the greatest slope and the feed direction. To pursue this analysis, a machining direction first needs to be defined that will be parameterized by the angle θ its projection makes in the plane (X, Y) with the axis X of the machine. Then a meshing of the parametric space comprising 256 x 256 tiles is considered. In the centre of each tile thus constituted, the effective radius of the torus milling cutter can be readily calculated using relation (30). The value of the effective radius thus obtained is then associated with a corresponding colour from a scale of colours varying linearly from r (blue) to $2R$ (red). The grid of colours is then applied as texture to the 3D representation of the surface to generate graphic images like those shown in figures 8 to 11.

The entire procedure (calculation and visualisation) was developed using the Java programming language.

4.4 Results

Here, the results for two cutters with outer radius $R = 5mm$ are presented. One cutter is a ball-end mill while the other is a torus milling cutter whose torus radius is $r = 2mm$. The surface considered is the extrados of a boat propeller as shown previously (section 4.1).

Applying the methodology defined in section 4.3 to a number of representative machining directions the following graphic representations are obtained:

- for a machining direction defined by $\theta = -45°$, figure 8 is obtained
- for a machining direction defined by $\theta = 0°$, figure 9 is obtained
- for a machining direction defined by $\theta = 45°$, figure 10 is obtained
- for a machining direction defined by $\theta = 90°$, figure 11 is obtained

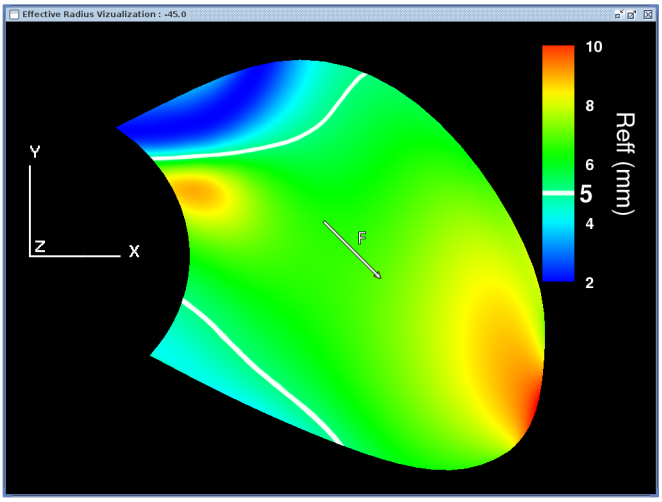

Figure 8: Visualisation of the effective radius for $\theta = -45°$

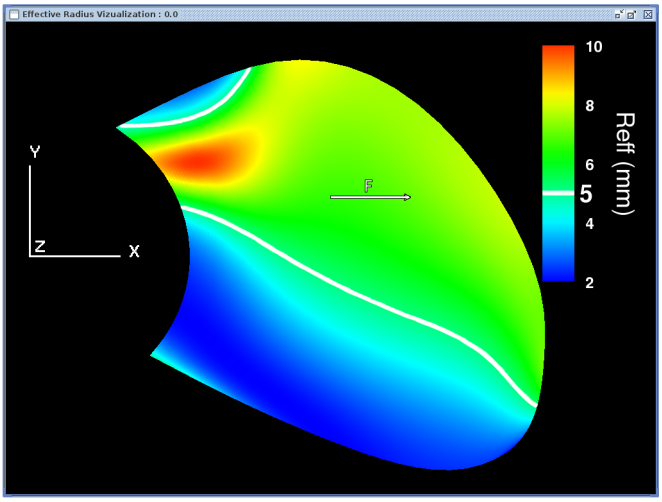

Figure 9: Visualisation of the effective radius for $\theta = 0°$

On these figures, the white curves represent the limit between the zones, that is the points where

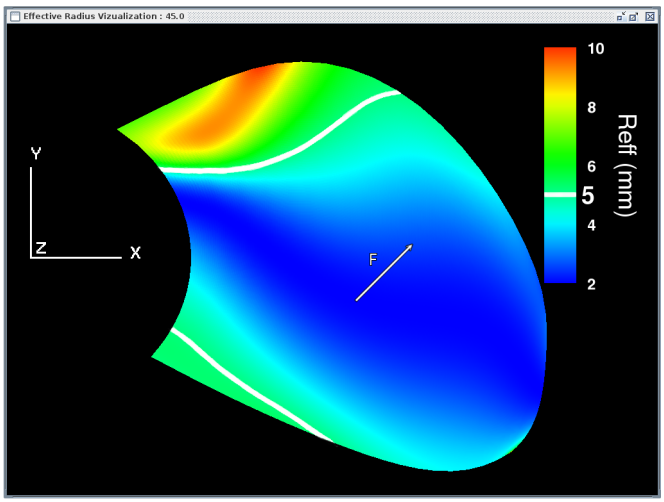

Figure 10: Visualisation of the effective radius for $\theta = 45°$

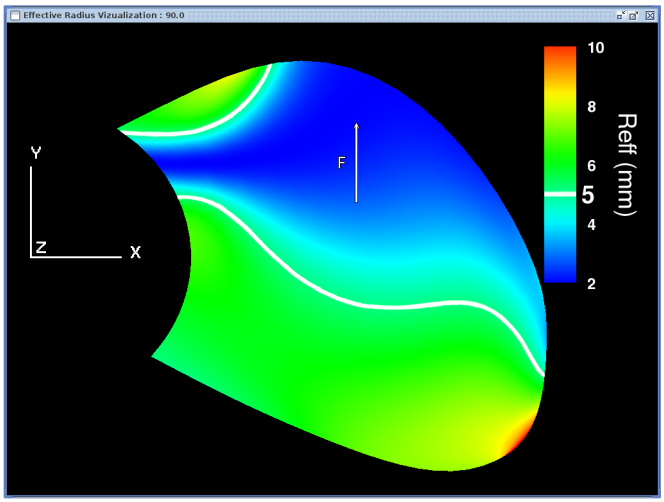

Figure 11: Visualisation of the effective radius for $\theta = 90°$

$R_{eff} = R = 5mm$. In the regions that are predominantly blue, $R_{eff} < R$ applies. It can thus be said that in these regions the ball-end mill is more effective than the torus milling cutter. Conversely, in mainly red and green regions, the effective radius of the torus milling cutter is greater than the nominal radius of the ball-end cutter ($R_{eff} > R$); as a result, it can be said that in these regions, the torus milling cutter is more effective than the ball-end cutter.

The calculation time needed to conduct the entire analysis procedure (computation and display) for all the tests conducted always took less than one second. This rapidity in calculation is essentially due to the simplicity of expression of the effective radius

(relation 30).

This simplicity of expression means that tools for analysis, like the one introduced here, can be defined to provide precious help in choosing a machining strategy.

5 Conclusions and perspectives

When end milling of free-form surfaces with a torus milling cutter, the effective radius concept is essential to analyse the machining procedure in purely geometrical terms.

The study presented in the present publication enabled the effective radius of a torus milling cutter milling with a translation movement to be expressed. Adopting this an original approach, this expression was determined in analytical form without having to resort to geometric approximation. This relation was also analysed and the limits to its validity were studied.

As the expression was relatively simple, it should pave the way for applications that it would be impossible to implement in a reasonable time frame using a numerical approach. As an example, a tool for numerical analysis was presented that could prove useful in pre-project analysis of a procedure for free-form machining using parallel planes.

The possibilities offered by the relation established in the present study are, however, far from being limited to the example adopted here. Due to it being so easy to implement, the analytical formula defined here to compute the effective radius may readily be integrated into recently developed "intelligent CAM" processes [24,25].

In forthcoming publications it will be seen how analytical expression of the cutter effective radius can find many different applications in studies into the machining of free-form surfaces with a torus milling cutter that adopt a geometric approach.

A Calculation detail

A.1 Identification of terms in r in equation (9)

From equation (13):

$$\frac{c\,\cos(t)}{\sqrt{b^2\sin^2(t)+c^2}} = \sqrt{1-\frac{c^2\sin^2(v)}{b^2\cos^2(v)}}\,\cos(v)$$

it can be deduced successively that:

$$\begin{aligned}
c^2\,\cos^2(t) &= \left(1-\frac{c^2}{b^2}\tan^2(v)\right)\cos^2(v)\,\left(b^2\,\sin^2(t)+c^2\right)\\
b^2\,c^2\,\cos^2(t)\,\left(1+\tan^2(v)\right) &= \left(b^2-c^2\tan^2(v)\right)\,\left(c^2+b^2\,\sin^2(t)\right)\\
&= b^2\,c^2+b^4\,\sin^2(t)-c^4\,\tan^2(v)-b^2\,c^2\,\tan^2(v)\,\left(1-\cos^2(t)\right)\\
b^2\,c^2\,\cos^2(t) &= b^2\,c^2+b^4\,\left(1-\cos^2(t)\right)-c^4\,\tan^2(v)-b^2\,c^2\,\tan^2(v)\\
b^2\,\cos^2(t)\,\left(b^2+c^2\right) &= b^2\,c^2+b^4-c^2\,\tan^2(v)\,\left(b^2+c^2\right)\\
\cos^2(t) &= c^2+b^2-\frac{c^2}{b^2}\,\tan^2(v)
\end{aligned}$$

and this leads to the following equation (12) :

$$\cos(t) = \sqrt{1-\frac{c^2\,\sin^2(v)}{b^2\,\cos^2(v)}}$$

A.2 Identification of terms in r in equation (10)

From equation (14) :

$$\frac{c\,\sin(t)}{\sqrt{b^2\,\sin^2(t)+c^2}} = -\left(\frac{c^3}{b}\,\sin(v)+b\,c\,\sin(v)\right)$$

it follows that:

$$\begin{aligned}\frac{c^2\,\sin^2(t)}{b^2\,\sin^2(t)+c^2} &= \left(\frac{c^3+b^2\,c}{b}\right)^2\,\sin^2(v)\\ &= \left(c^2+b^2\right)^2\,\frac{c^2}{b^2}\,\sin^2(v)\end{aligned}$$

whence

$$\begin{aligned}b^2c^2\sin^2(t) &= c^2\sin^2(v)\left(b^2\sin^2(t)+c^2\right)\\ b^2\,c^2\,\sin^2(t)\,\left(1-\sin^2(v)\right) &= c^4\,\sin^2(v)\\ b^2\,\sin^2(t)\,\cos^2(v) &= c^2\,\sin^2(v)\\ 1-\cos^2(t) &= \frac{c^2\,\sin^2(v)}{b^2\,\cos^2(v)}\end{aligned}$$

from which follows equation (12) :

$$\cos(t)=\sqrt{1-\frac{c^2\,\sin^2(v)}{b^2\,\cos^2(v)}}$$

References

[1] Ali Lasemi, Deyi Xue, and Peihua Gu. Recent development in CNC machining of freeform surfaces: A state-of-the-art review. *Computer-Aided Design*, 42(7):641–654, Juil 2010.

[2] G.W. Vickers and K.W. Quan. Ball-mills versus end-mills for curved surface machining. *Journal of Engineering for Industry — Transactions of the ASME*, 111(1):22–26, Fév 1989.

[3] W.L.R. Ip and M. Loftus. Cusp geometry analysis in free-form surface machining. *International Journal of Production Research*, 30(11):2697–2711, Nov 1992.

[4] H.D. Cho, Y.T. Jun, and M.Y. Yang. 5-axis CNC milling for effective machining of sculptured surfaces. *International Journal of Production Research*, 31(11):2559– 2573, Nov 1993.

[5] B.H. Kim and C.N. Chu. Effect of cutter mark on surface roughness and scallop height in sculptured surface machining. *Computer-Aided Design*, 26(3):179–188, Mar 1994.

[6] S. Bedi, F. Ismail, M. J. Mahjoob, and Y. Chen. Toroidal versus ball nose and flat bottom end mills. *The International Journal of Advanced Manufacturing Technology*, 13(5):326–332, 1997.

[7] C. G. Jensen and D. C. Anderson. Accurate tool placement and orientation for finished surface machining. *Journal of Design and Manufacture*, 3:251–261, 1993.

[8] Jean-Max Redonnet, Walter Rubio, Frédéric Monies, and Gilles Dessein. Optimising tool positioning for end-mill machining of free-form surfaces on 5-axis machines for both semi-finishing and finishing. *The International Journal of Advanced Manufacturing Technology*, 16(6):383–391, Mai 2000.

[9] Yuan-Shin Lee. Admissible tool orientation control of gouging avoidance for 5-axis complex surface machining. *Computer-Aided Design*, 29(7):507–521, Juil 1997.

[10] Frédéric Monies, Michel Mousseigne, Jean-Max Redonnet, and Walter Rubio. Determining a collision-free domain for the tool in five-axis machining. *International Journal of Production Research*, 42(21):4513–4530, Nov 2004.

[11] Khalid Sheltami, Sanjeev Bedi, and Fathy Ismail. Swept volumes of toroidal cutters using generating curves. *International Journal of Machine Tools and Manufacture*, 38(7):855–870, Juil 1998.

[12] Yun C. Chung, Jung W. Park, Hayong Shin, and Byoung K. Choi. Modeling the surface

swept by a generalized cutter for NC verification. *Computer-Aided Design*, 30(8):587–594, Juil 1998.

[13] Seok Won Lee and Andreas Nestler. Complete swept volume generation, part I: Swept volume of a piecewise C1-continuous cutter at five-axis milling via gauss map. *Computer-Aided Design*, 43(4):427–441, Avr 2011.

[14] C. J. Chiou and Y. S. Lee. Swept surface determination for five-axis numerical control machining. *International Journal of Machine Tools and Manufacture*, 42(14):1497–1507, Nov 2002.

[15] D. Roth, S. Bedi, F. Ismail, and S. Mann. Surface swept by a toroidal cutter during 5-axis machining. *Computer-Aided Design*, 33(1):57–63, Jan 2001.

[16] Stephen Mann and Sanjeev Bedi. Generalization of the imprint method to general surfaces of revolution for nc machining. *Computer-Aided Design*, 34(5):373– 378, Avr 2002.

[17] K. Suresh and D.C.H. Yang. Constant scallop-height machining of free-form surfaces. *Journal of Engineering for Industry — Transactions of the ASME*, 116(2):253–259, Mai 1994.

[18] R. S. Lin and Y. Koren. Efficient tool-path planning for machining free-form surfaces. *Journal of Engineering for Industry — Transactions of the ASME*, 118(1):20–28, Fév 1996.

[19] Yuan-Shin Lee. Non-isoparametric tool path planning by machining strip evaluation for 5-axis sculptured surface machining. *Computer-Aided Design*, 30(7):559–570, Juin 1998.

[20] A Can and A Ünüvar. A novel iso-scallop toolpath generation for efficient five-axis machining of free-form surfaces. *The International Journal of Advanced Manufacturing Technology*, 51(9-12):1083–1098, December 2010.

[21] Z.C. Chen and D. Song. A practical approach to generating accurate iso-cusped tool paths for three axis cnc milling of sculptured surface parts. *Journal of Manufacturing Processes*, 8(1):29–38, 2006.

[22] Jianxin Pi, Edward Red, and Greg Jensen. Grind-free tool path generation for five-axis surface machining. *Computer Integrated Manufacturing Systems*, 11(4):337–350, Oct 1998.

[23] Maxima. a computer algebra system. version 5.26.0, 2012.

[24] C. Manav, H.S. Bank, and I. Lazoglu. Intelligent toolpath selection via multi-criteria optimization in complex sculptured surface milling. *Journal of Intelligent Manufacturing*, pages 1–7, 2011.

[25] L.N López de Lacalle, A. Lamikiz, J. Muñoa, and J.A. Sánchez. The CAM as the centre of gravity of the five-axis high speed milling of complex parts. *International Journal of Production Research*, 43(10):1983–1999, 2005.